Effect of Air Shear on Gas Absorption by a Liquid Film

Rates of oxygen absorption from turbulent air by a concurrently flowing liquid film were measured in an enclosed 2.54 cm × 30.5 cm rectangular channel. The effect of liquid viscosity is varied by using water and a water-glycerine solution. The results are interpreted by arguing that flow fluctuations in the liquid that control mass transfer are associated with waves of small wavelength at the interface.

M. J. McCREADY

and T. J. HANRATTY

Department of Chemical Engineering
University of Illinois
Urbana, IL 61801

SCOPE

Gas absorption rates of a liquid layer are greatly enhanced by the presence of interfacial shear. Mass transfer coefficients for concurrent gas-liquid flows can be several times larger than those for liquid films that are freely falling down a vertical or inclined wall. The reasons for this are not completely understood. This paper presents results for oxygen absorption under carefully controlled conditions with the goal of investigating the role of an air flow in enhancing transfer rates. Particular insights were gained by varying the liquid viscosity and by accompanying the absorption measurements with measurements of wave properties, interfacial stress, and liquid phase turbulence.

Our work was motivated to a large extent by a previous study made by Henstock and Hanratty (1979) in this laboratory. From experiments with water films, they correlated absorption results for a freely falling film (zero gas flow) with the equation

$$K^+ = 0.0077 m^{+1/2} Sc^{-1/2}. \quad (1)$$

Here K^+ and m^+ are the mass transfer coefficient and the film height, made dimensionless with the friction velocity and the kinematic viscosity, and Sc is the Schmidt number. The rate expression for nonzero gas flow is, in general, quite different from Eq. 1. However, Henstock and Hanratty (Eq. 43 in the cited paper) suggested that at high ratios of the gas to liquid flow rate gas shear controlled mass transfer; the rate then is given by a relation of the same form as Eq. 1 for air and water flowing concurrently downward:

$$K^+ = 0.0216 m^{+1/2} Sc^{-1/2}. \quad (2)$$

The present experiments, which are an extension of preliminary work reported by Henstock and Hanratty, allow for the study of oxygen absorption under conditions in which gas shear is completely controlling. They reveal a behavior quite different from Eq. 2.

CONCLUSIONS AND SIGNIFICANCE

Henstock and Hanratty (1979) argued that turbulence in the liquid controlled mass transfer. Such an interpretation cannot explain the observed effect of liquid flow rate and, in particular, of liquid viscosity on the absorption rate. A more fruitful approach is to relate mass transfer to system variables through their effect on wave properties. A promising theoretical explanation of the effect of waves is that they induce spatial variations of interfacial drag that agitate the liquid close to the interface.

INTRODUCTION

The major resistance to the absorption of a slightly soluble gas is in the liquid phase. Because of the large Schmidt number characterizing the process, all of the concentration change in the liquid occurs in a very thin region. Therefore, mass transfer is controlled by fluctuations in the liquid so close to the interface that the velocity components can be described by the first terms of Taylor series expansions in distance from the interface. There are three possible sources for these fluctuations: turbulence generated in the liquid, induced flows associated with surface waves, and gas flow turbulence. The theoretical problem is to determine the relative importance of these sources and to relate mass transfer rates to the properties of the fluctuating velocity.

In the experiments described in this paper, air and a liquid flowed concurrently in a 2.54 cm × 30.5 cm rectangular chan-

M. J. McCready is presently with the Department of Chemical Engineering, Notre Dame University, Notre Dame, Indiana.

nel. Rates of oxygen absorption were determined by sampling the liquid at different locations along the channel length. Effects of liquid viscosity were studied by using water and a 20% glycerine-water mixture with a viscosity approximately twice that of water. The interfacial stress was determined from pressure drop and velocity measurements in the gas and wave properties by means of a conductance probe. Measurements of wall shear stress fluctuations gave an indication of turbulence in the liquid and, for very thin films, showed that gas phase turbulence can affect the film. The range of variables studied was such that a three-dimensional pebbled wave pattern existed at the interface.

While mass transfer rates to free-falling films are well characterized, relatively few results are available for sheared gas-liquid interfaces. Kamei and Oishi (1955), Chung and Mills (1974), Henstock and Hanratty (1979) studied oxygen absorption by sheared films flowing down the inside wall of a pipe. In these experiments the height of these films is quite small and the interface is dominated by long-wavelength disturbance or "roll waves." The experiments by Mattingly (1977) and by Tsacoyaninis (1976) appear much closer to those described in this paper in that they involve air-water flows in 55 cm × 55 cm and 10 cm × 20 cm horizontal, rectangular channels. These systems are larger than the one used by us and the large wavelength waves are quite different. It is therefore of considerable interest to compare our measurements with theirs.

Measurements of velocity fluctuations have been carried out as close as possible (about 5 mm) to a sheared interface by Suzanne (1977). These indicate that turbulent intensities are much larger than are found near unsheared interfaces. However, the waviness of the surface prevented measurements close enough to the interface to study velocity fluctuations that control mass transfer.

Waves at an interface induce a spatial variation of the air flow and of the drag of the gas at the interface. As has been shown in a number of previous papers from this laboratory (Thorsness et al., 1978; Hanratty, 1983; Abrams, 1984), the amplitude of these shear stress variations can be quite large (compared to the average shear stress) for small wavelength waves. This spatial shear stress variation is coupled through liquid viscosity to a cellular motion in the liquid close to interface of the type shown in Figure 1, which, we will argue, could strongly affect mass transfer rates. A discussion of the relation of the magnitude of the activity in this cell to wave properties is presented in the next section.

EFFECT OF WAVES

To determine the magnitude of flows within the liquid an idealized regular wave pattern is used. This should give a satisfactory representation of the small wavelength waves that actually occur at the interface.

Consider a wavelike sinusoidal disturbance at the interface of a liquid film of thickness m of the form

$$\eta = a \exp[i\alpha(x - Ct)], \tag{3}$$

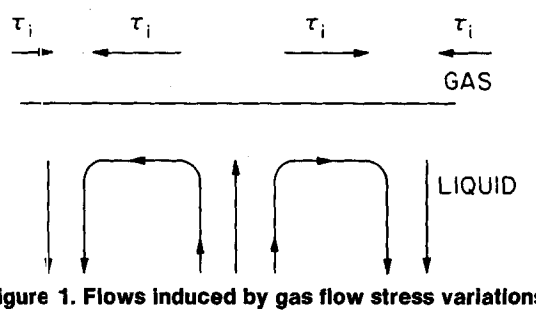

Figure 1. Flows induced by gas flow stress variations.

where the wave number, α, the amplitude, a, and the velocity, C, are real numbers. This disturbance is accompanied by velocity fluctuations given by

$$u = \hat{u} \exp[i\alpha(x - Ct)], \tag{4}$$

$$v = \hat{v} \exp[i\alpha(x - Ct)], \tag{5}$$

where the complex amplitudes $\hat{u}(z)$ and $\hat{v}(y)$ are functions of the distance from the average location of the interface, y. From conservation of mass,

$$i\alpha\hat{u} + \frac{d\hat{v}}{dy} = 0. \tag{6}$$

For small-amplitude waves the velocity component in the y direction, v, is given by the linearized form of the momentum balance equation,

$$(U - C)\left(\frac{d^2\hat{v}}{dy^2} - \alpha^2\hat{v}\right) - \frac{d^2U}{dy^2}\hat{v} = \frac{1}{i\alpha Re}\left(\frac{d^4\hat{v}}{dy^4} - 2a^2\frac{d^2\hat{v}}{dy^2} + \alpha^4\hat{v}\right), \tag{7}$$

where U is the average velocity in the liquid.

All the variables in Eqs. 6 and 7 have been made dimensionless using m, U_o, the spatial average value of U, and ν, the kinematic viscosity of the liquid, so that $Re = mU_o/\nu$.

The boundary conditions to be satisfied at the interface are the kinematic condition,

$$\frac{\partial\eta}{\partial t} + U_s\frac{\partial\eta}{\partial x} = v_s \tag{8}$$

and the equality of stresses in the gas and liquid,

$$\hat{\tau}_s = \frac{1}{Re}\left(\frac{\partial u}{\partial y} + \frac{\partial v}{\partial x}\right)_s. \tag{9}$$

Here, τ_s, the shear stress exerted by the gas on the liquid, is given by

$$\tau_s = \bar{\tau}_o + \hat{\tau}_s \exp[i\alpha(x - Ct)], \tag{10}$$

where $\hat{\tau}_s$ is the complex amplitude of the wave-induced stress variation. The other two conditions to be satisfied are that $u = v = 0$ at the solid boundary.

For small amplitude waves and for large αRe, the following solution to Eq. 7 is obtained:

$$\hat{v} - \hat{v}_s = \frac{\alpha(U_\rho - C) + D}{[(1 - (e^\alpha/e^{-1})]}\left[e^{-\alpha y} - \frac{e^\alpha}{e^{-\alpha}}e^{\alpha y}\right] + D\exp\left[\sqrt{i(U_o - C)\alpha Re}\, y\right] - i\alpha(U_o - C)a, \tag{11}$$

where

$$D = -\frac{\hat{\tau}_s Re + 2\alpha^2 a(U_o - C)}{(U_o - C)Re + i\alpha} \tag{12}$$

For large values of αRe and relatively thick films, Eq. 11 can be written in the following form for $y \to 0$:

$$\hat{v} - \hat{v}_s = -\frac{y\hat{\tau}_s\sqrt{\alpha Re}}{[(C - U_o)]^{1/2}} \tag{13}$$

Mass transfer is controlled by fluid velocity relative to the motion of the interface. Consequently the relative amplitude of the normal velocity fluctuations, $(\hat{v} - \hat{v}_s)$, is considered in Eq. 13, rather than the amplitude $\hat{v}$. Values of the amplitude, $|\hat{v} - \hat{v}_s|$, calculated from Eq. 11 are plotted in Figure 2 using actual experimental values for a relatively thick liquid layer, $m^+ = 90$, and in

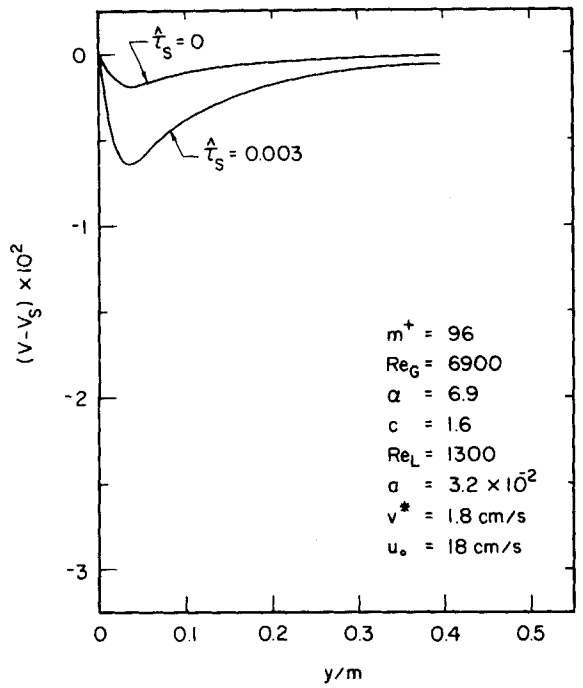

Figure 2. Magnitude of wave-induced normal velocities, relative to the interface velocity, for a thin liquid film.

Figure 3 for a thin liquid layer, $m^+ = 14$. Of particular interest is $d|\hat{v} - \hat{v}_s|/dy$ for $y \to 0$, since, as shown by McCready (1984), this is the hydrodynamic variable of primary interest.

The main feature to be noted in Figures 2 and 3 is that the gradient of normal velocity is much greater for a stressed interface ($\hat{\tau}_s \neq 0$) than for a free interface ($\hat{\tau}_s = 0$). This points out a mechanism whereby waves can enhance mass transfer: Waves by themselves do not create large relative velocities. However, waves in the presence of an air flow induce a spatial variation of the shear stress which has associated with it a cellular motion in the liquid of the type shown in Figure 1. This type of cellular motion is able to agitate the liquid in the immediate vicinity of the interface and, thereby, to create large normal fluid motions relative to the interfacial motion.

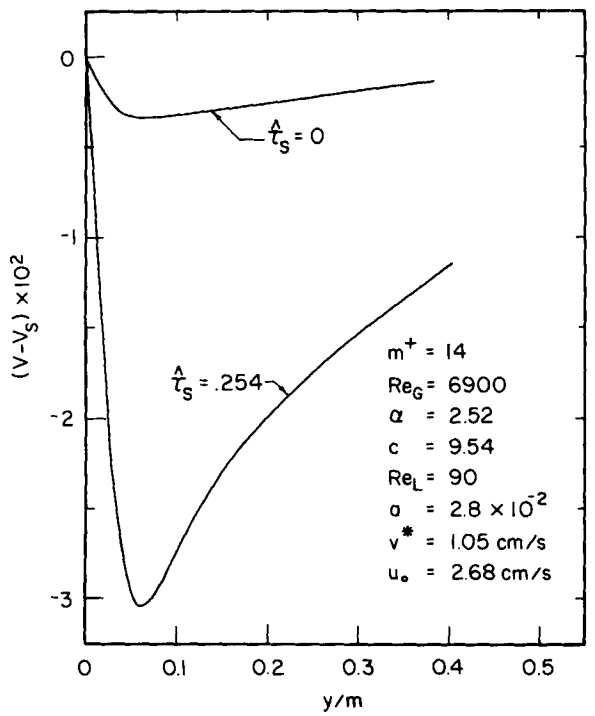

Figure 3. Magnitude of wave-induced normal velocities, relative to the interface velocity, for a thin liquid film.

DESCRIPTION OF EXPERIMENTS

Flow System

The gas-liquid flow system, which has been described previously by Miya (1970), is a Plexiglas, horizontal channel 2.54 cm high, 30.5 cm wide, and approximately 10 m long. Filtered and humidified air is supplied by a blower to the front end of the channel. Liquid is pumped into the bottom of the channel through a screen to minimize flow disturbances. This type of entry section allows the development of the wave field within about 0.5 m; measurements of hydrodynamics and mass transfer rates were made farther down the channel.

The water for the gas absorption measurements was used once and discarded. The glycerine solution, which was recycled, was deaerated by pulling it through a partially open valve with a centrifugal pump. At the point of cavitation the dissolved gas forms air bubbles. The bubbly liquid is fed to a surge tank where the bubbles rise to the surface before they can redissolve. The solution was covered and filtered to prevent the accumulation of contaminants. More details about the air removal system are given by McCready (1984) and Maxwell (1969).

Mass Transfer Measurements

The mass transfer coefficients were determined by measuring the average oxygen concentration of the liquid film at two locations between 1.5 and 3 m apart in the flow direction, as shown in Figure 4. Sample streams were withdrawn through the bottom of the channel by using hypodermic needles. Two tests were carried out to insure that the samples were representative of the bulk concentration. They showed:

(1) Dye injected into the flowing liquid film was found to disperse rapidly for all experimental conditions.

(2) No differences in concentration were noted when the needles were traversed vertically within the film.

The O_2 concentration was monitored continuously using flow cells with polarographic electrodes, as described by Henstock (1977). The equation used to calculate K, the mass transfer coefficient, is

$$K = \frac{\Gamma}{L} \ln\left(\frac{c_1 - c^*}{c_2 - c^*}\right), \tag{14}$$

where Γ is the flow rate per unit width, L is the distance between the sampling points, c_1 and c_2 are the corresponding O_2 concentrations, and c^* is the equilibrium O_2 concentration at the interface. The polarographic technique allows accurate determination of percent saturation for fluids of different composition and temperature so that the exact value of the equilibrium oxygen concentration is not needed. Individual runs were done at constant gas Reynolds number by decreasing the liquid flow from its maximum value. Variations in the liquid rate cause much larger changes in mass transfer rates than do changes in gas velocity.

Wave Measurements

The properties of the surface waves were measured over the same range of flow conditions as the mass transfer rates, using a parallel wire conductance probe. It consisted of two (0.15 mm) platinum wires that were strung through the bottom of the channel and placed 1.6 mm apart in the transverse direction (Figure 4). The wires were held taut by weights pulling down across a horizontal rod. A complete description of this type of probe is given by Miya (1970).

The film height is proportional to the electrical conductance between the wires, which is determined continuously by using an electronic analyzer. The probe and analyzer are capable of resolving waves with frequencies up to about 250 Hz.

The fluctuating output voltage of the film height analyzer was low pass filtered at 250 Hz, using an analog filter, and sampled using a LSI 11/23 microcomputer with a Data Translation DT1762 A/D converter at 500

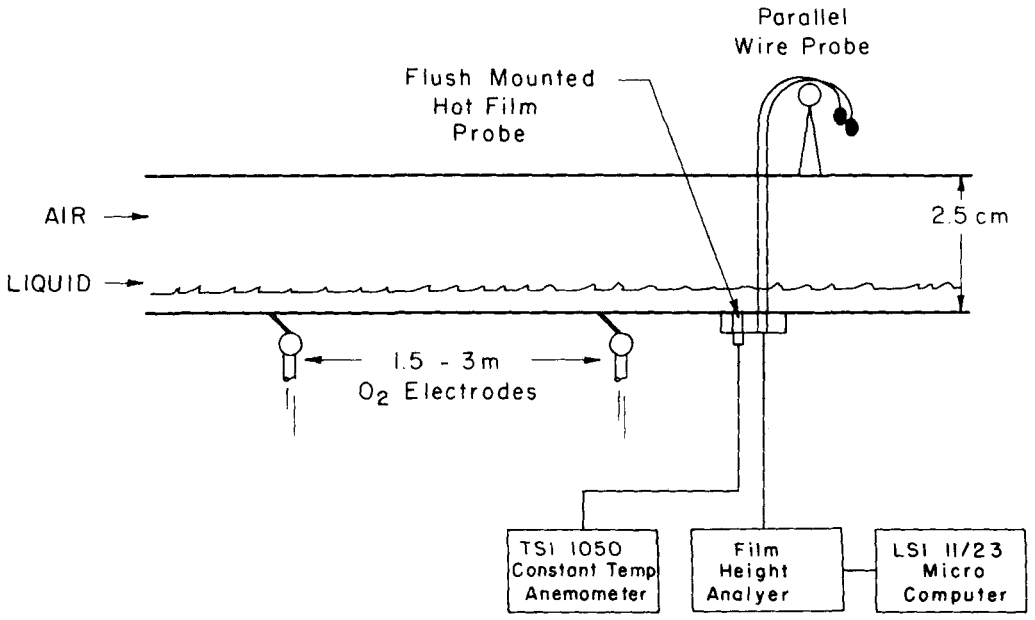

Figure 4. The measuring system.

samples/s to prevent any chance of aliasing. A total of 60,000 data points were taken for each set of conditions. More details about data sampling are given by McCready (1984).

The surface displacement spectra were calculated with a Fast Fourier Transform routine which used 20,480 points with 256 in each window.

The parallel wire probes were calibrated using the contact probe and circuit described by Henstock (1977). The probe was traversed vertically across the channel to determine the percent of contact time position. The average film height is then calculated from

$$\bar{h} = m = \int_0^\infty hP(h)dh, \tag{15}$$

where $P(h)$ is the probability density function.

Wall Shear Stress

The wall shear stress below the liquid film was measured using a flush-mounted hot film probe (TSI 1237W), as described by Miya (1970). The fluctuating shear stress signal was sampled and stored in the same manner as the wave analyzer output. This information is only useful for qualitative comparison because the probe was not calibrated to match the average wall stress.

Other Measurements

The average pressure drop over about a meter of the channel was measured using a micromanometer. In addition, gas phase velocity profiles were determined with a pitot tube. The average stress at the gas-liquid interface could then be determined because the stress varies linearly from the point of zero stress. Because of the roughness of the wavy surface, the point of zero stress corresponds only roughly to the maximum in velocity. The exact point of zero stress was determined by using results reported by Miya (1970) that relate the point of maximum velocity to the point of zero stress. Generally, the zero stress point occurs at about two-thirds of the distance between the interface and the velocity maximum.

RESULTS

Mass Transfer Results

Mass transfer coefficients for oxygen absorption into water are plotted in Figure 5. Two regions are identified: For $m^+ < 40$, $KSc^{1/2}/v^*$ decreases rapidly with decreasing m^+, indicating a strong dependence on film height. However, for $m^+ > 40$, $KSc^{1/2}/v^*$ is approximately constant at a value of 0.17. The observation for thick films that K^+ is a function only of Schmidt number is similar to what is found for turbulent mass transfer to a solid boundary.

Data obtained by Tsacoyannis for much thicker films (1–3 cm) are also shown in Figure 5. Again $KSc^{1/2}/v^*$ is found to be roughly constant, but with a slightly lower value than what was found in our experiments.

Absorption rates for a 20% glycerine-water solution are given

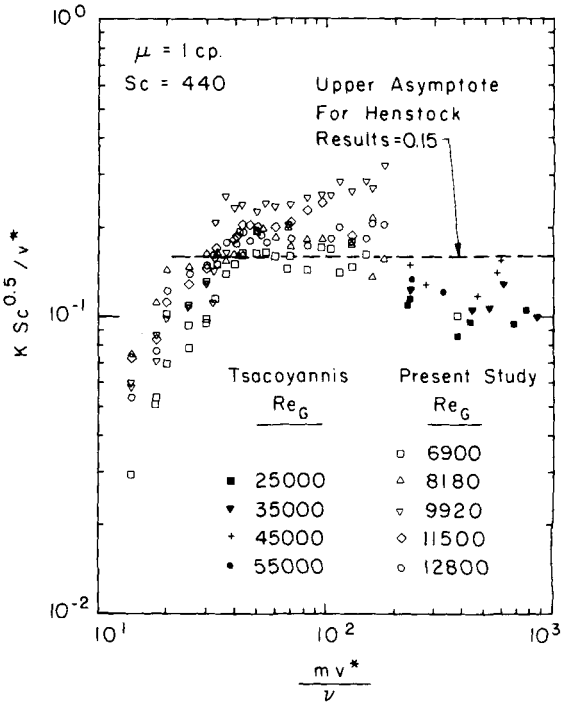

Figure 5. Mass transfer coefficients for oxygen absorption by a water film.

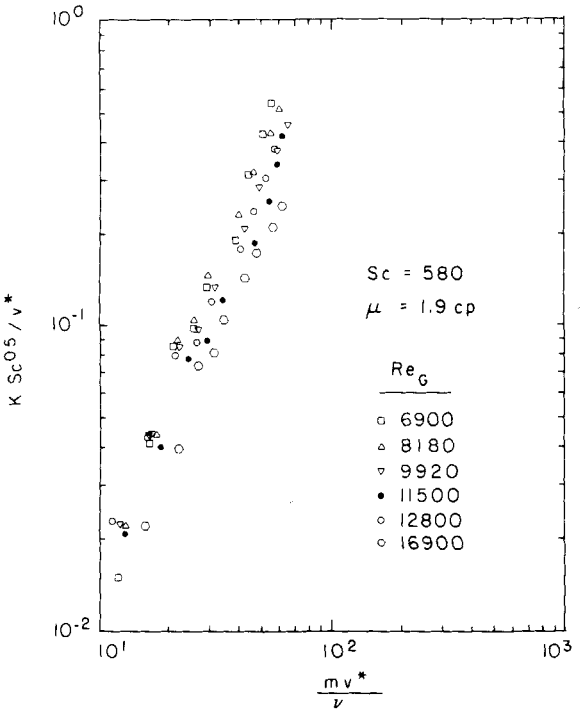

Figure 6. Mass transfer coefficients for oxygen absorption by a glycerine-water solution with a viscosity of 1.9 cp (mPaos).

in Figure 6. These exhibit a behavior that is different from the water data. The dimensionless mass transfer rate is a strong function of m^+ over the whole range that was studied, $m^+ < 70$. It is quite possible that a region of constant K^+ would be observed for larger film thickness, but it was not possible to carry the experiments into this range of variables since slugging was observed to occur for $m^+ > 70$.

It is also to be noted that for $m^+ > 50$ values of $KS^{1/2}/v^*$ are significantly larger than what is measured for water. This behavior was unexpected since it is inconsistent with existing theories. Some help in understanding this difference is obtained when wave properties of the two liquids are examined.

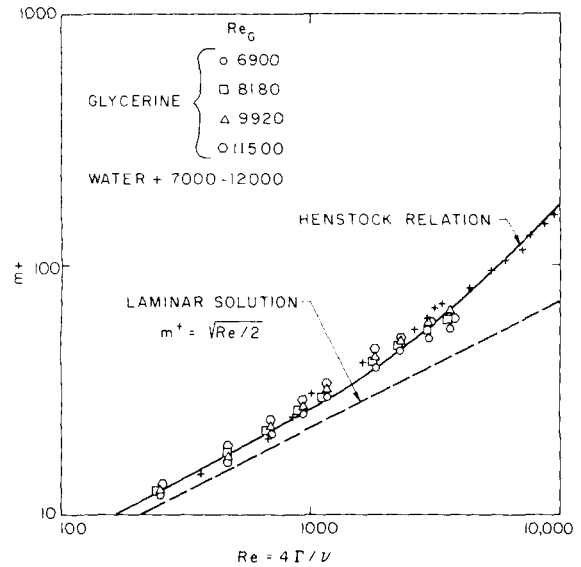

Figure 7. Film height measurements for water and water-glycerine solutions with a viscosity of 1.9 cp (mPaos).

Average Film Heights

A plot of the dimensionless height, m^+, vs. Reynolds number, defined as $4\Gamma/\nu$, is given in Figure 7. Measurements for water and for glycerine-water collapse on a single curve when plotted in this fashion. The dashed line is the laminar flow solution, $m^+ = (Re/2)^{1/2}$. The data are only slightly higher than this relation at small flow rates. At large flow rates the data diverge from the laminar flow relation and become more turbulent. The solid curve is an interpolation formula, presented by Henstock and Hanratty (1976), that gives laminar and turbulent flow in the limits of $Re \to 0$ and $Re \to \infty$:

$$m^+ = [(0.707Re^{1/2}/\ )^{2.5} + (0.0379\ Re^{0.90})^{2.5}]^{0.40} \qquad (16)$$

Surface Waves

Typical surface height measurements are shown in the top part of Figure 8. A fluctuating film height is defined as

$$h' = h - m. \qquad (17)$$

The wave height is characterized as the time mean of the square of the film height fluctuations, $\overline{h'^2}$. A wave spectral function, $W_h(n)$, defined as

$$\overline{h'^2} = \int_0^\infty W_h(n)dn, \qquad (18)$$

gives the contribution of different frequencies to the wave height.

Measurements of the wave spectral function for air and water are presented in Figure 9 for a constant gas Reynolds number of 6,900. Here $Re_G = (B - m)V_G/\nu_G$, with B signifying the channel height (2.54 cm). Spectra for different liquid flow rates have the same basic shape. The spectral function increases to a peak, between 10 and 20 Hz, and then decreases for higher frequencies. The frequency at which this peak occurs represents the dominant waves with a wavelength of about 2 cm that are observed visually. They are three-dimensional, having a width of the same order as the length. The number of large-amplitude fluctuations per unit time shown in Figure 8 corresponds roughly to this peak frequency.

If waves are controlling mass transfer, they must cause flow fluctuations very close to the interface. For this reason, waves of shorter length and higher frequency are of greater interest than the dominant ones. For the case in which h' is given by a Gaussian distribution, the number of maxima per unit time is given by

$$N(h_m) = \left[\frac{\int_0^\infty n^4 W_h(n)dn}{\int_0^\infty n^2 W_h(n)dn}\right]^{1/2} \qquad (19)$$

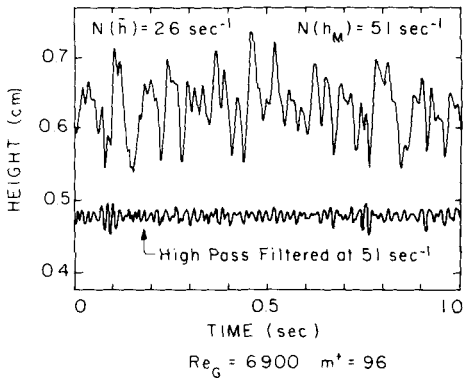

Figure 8. Unfiltered and filtered film height tracings for a water film at Re_G = 6,900 and $m+$ = 96.

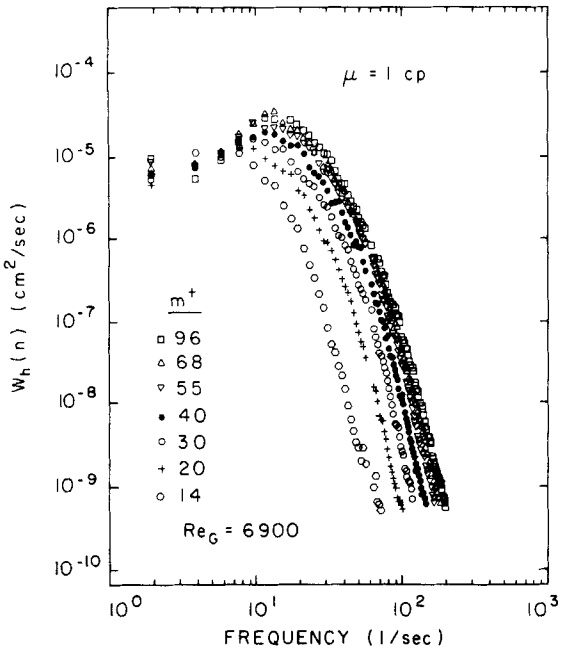

Figure 9. Effect of film flow rate on frequency spectra of waves at an air-water interface.

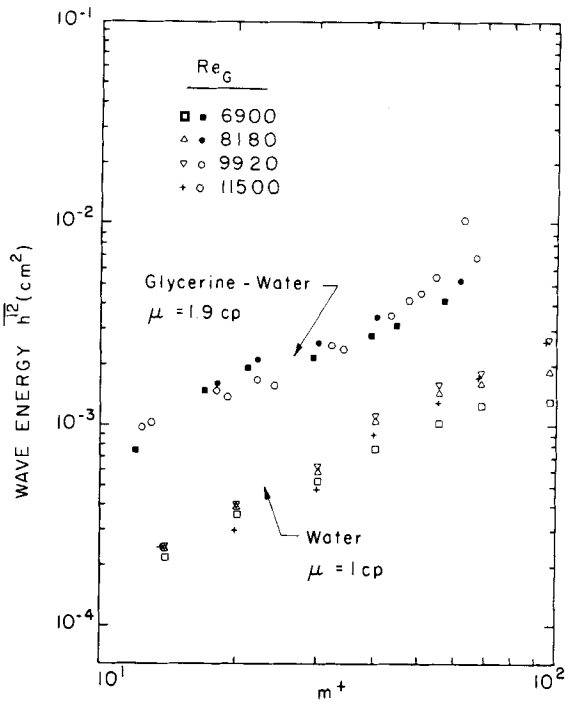

Figure 10. Mean-square wave heights for water films and for water-glycerine films of 1.9 cp (mPaos).

and the number of zero crossings is given by

$$N(\bar{h}) = \left[\frac{\int_o^\infty n^2 W_h(n)dn}{\int_o^\infty W_h(n)dn}\right]^{1/2} . \qquad (20)$$

The filtered signal shown in Figure 8 was obtained by removing all frequencies lower than $N(h_m)$. It is noted that this signal contains all the peaks shown in the unfiltered signal, but has much lower energy.

Values of $N(h_m)$ and $N(\bar{h})$ calculated from the spectra shown in Figure 9 are summarized in Table 1. The frequency of maxima is about four times the frequency corresponding to the peak value of W_h for large m^+, and about five times the peak frequency for $m^+ = 14$. It corresponds to the high-frequency region of the spectra in Figure 9, which contains a small fraction of the total wave energy. It is noted in Figure 9 that the spectra, and in particular the high-frequency portion, are strongly affected by m^+ for $m^+ < 40$ and appear to be reaching an asymptotic behavior for $m^+ > 40$. This is illustrated in Figure 10 where $\overline{h'^2}$ is plotted against m^+ for the data shown in Figure 9 and for air-water results at other gas Reynolds numbers. It is noted that the wave energy increases with v^* and that there is sharp change in the slope of the relations between the wave energy and m^+ beyond $m^+ \doteq 40$. This is qualitatively similar to the change in character of the relation between K and v^* for $m^+ > 40$.

Spectral data for the glycerine-water are shown in Figure 11 for the same gas Reynolds number as the data shown in Figure 9. The shapes of the spectral functions are the same as were observed for water. These films are thicker than the water films and the waves are of larger magnitude. A saturation condition for the high-frequency portion of the spectral function is not observed in the range of measurements. If saturation does eventually occur, it must be at values of m^+ much larger than 40.

Measured values of $N(h_m)$ and $\overline{h'^2}$ for the glycerine-water solutions are summarized in Table 1. A plot of $\overline{h'^2}$ vs. m^+ is given in Figure 10. It is noted that the wave energy for the glycerine-water solution increases with increasing m^+ for the entire range of m^+ that was investigated, similar to what has been observed for the mass transfer data shown in Figure 6. It is also to be noted that values of $\overline{h'^2}$ are obtained for $m^+ > 40$, which are larger than observed for water. This correlates quite nicely with the larger values of $KSc^{0.5}/v^*$ observed for the glycerine solution.

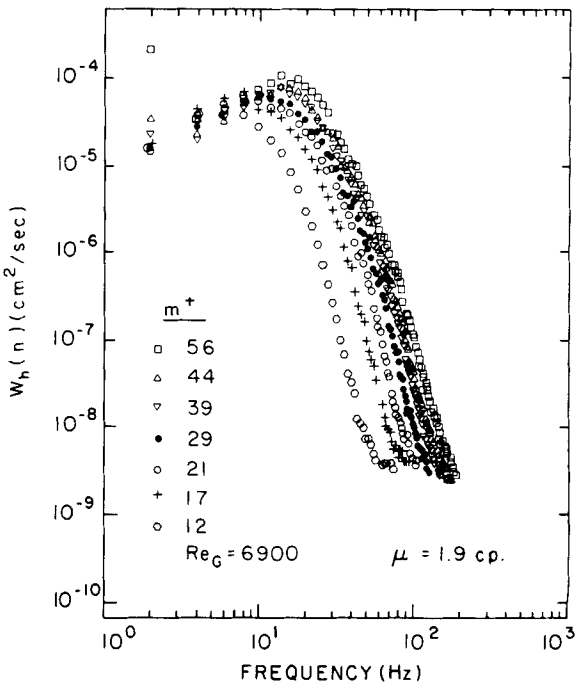

Figure 11. Effect of film flow rate on frequency spectra of waves at the interface of an air flow and a glycerine-water film of viscosity 1.9 cp (mPaos).

Table 1. Statistical Properties of the Waves

m^+	Re_G	$\bar{m}$ cm	$(m-\bar{m})^2$ $cm^2 \times 10^4$	Freq. of Zero Crossings s^{-1}	Freq. of Maxima s^{-1}	Freq. at Maxima of Spectral Function s^{-1}
			Water:			
96	6,900	0.620	13.2	26.5	51.3	10
68	6,900	0.541	12.5	24.3	48.0	13
55	6,900	0.500	10.2	24.3	46.3	13
40	6,900	0.422	7.61	22.4	42.2	11
30	6,900	0.356	5.27	20.0	37.9	10
20	6,900	0.320	3.58	16.7	33.7	9
14	6,900	0.284	2.18	13.1	35.8	7
			Glycerine Solution:			
56	6,900	0.767	70.3	23.1	43.5	16
44	6,900	0.625	38.1	21.8	39.7	14
39	6,900	0.559	29.0	21.2	37.8	14
29	6,900	0.437	23.1	19.3	33.7	12
21	6,900	0.330	20.5	16.8	28.6	10
17	6,900	0.269	16.8	14.2	24.1	8
12	6,900	0.206	8.71	10.5	17.2	5

Wall Shear Stress Measurements

Tracings of simultaneous measurements of the fluctuating wall shear stress and the fluctuating film height are shown in Figure 12. For the thickest films there is a high degree of correlation between the shear stress and the wave signals. Dominant waves are seen at the wall as shear stress fluctuations.

As the liquid flow rate is reduced, the degree of correlation between the film height and wall shear stress fluctuations decreases. However, even though the energy in the high-frequency waves decreases, the wall shear stress continues to show high-frequency fluctuations. It appears that shear stress variations caused by turbulence in the gas flow penetrate far enough into the liquid to be detected by the flush-mounted film probe at the wall.

Further evidence of the influence of gas flow turbulence on liquid velocity fluctuations is shown in Figure 13. Wave and shear stress spectra are observed to decrease smoothly above 20 Hz. However, for thin films the shear stress spectra show a local maximum at a frequency of 40 Hz. This corresponds roughly to what would be expected for the frequency of gas phase shear stress fluctuations (Hanratty et al., 1977).

The wall shear stress tracings indicate no clear transition from laminar to turbulent flow. The effects of the waves and the gas flow turbulence cause all signals to appear turbulent. Thus, this type of measurement does not appear to be effective in determining which type of fluctuations are controlling mass transfer.

COMPARISON WITH VERTICAL FLOW RESULTS

The results obtained in this research suggested that the absorption measurements obtained by Henstock and Hanratty (1979) for air-water flow down a vertical pipe be replotted in the manner

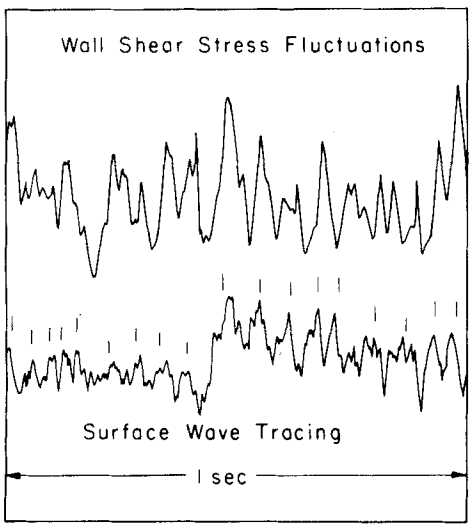

Figure 12. Tracings of the time variation of the film height and of the wall shear stress.

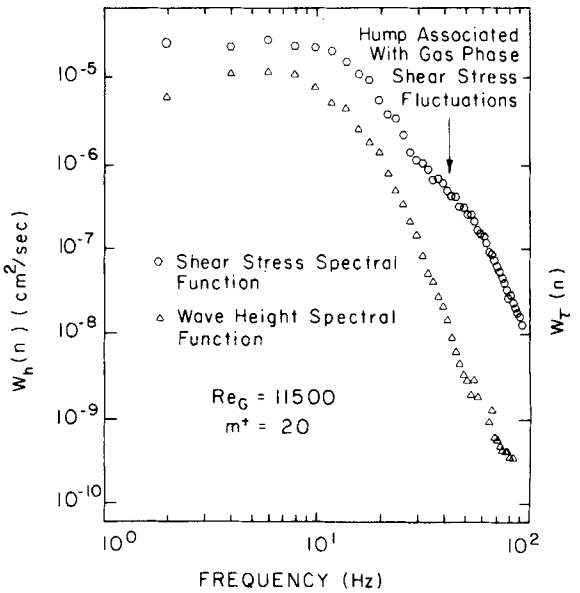

Figure 13. Comparison of spectral functions for the film height and the wall shear stress fluctuations for air-water flow.

shown in Figure 14. It is noted that a line

$$K^+Sc^{1/2} = 0.15 \tag{21}$$

represents an upper asymptote for the data for large ratios of the gas-to-liquid flow rate. This is in remarkably good agreement with results shown in Figure 5 for a horizontal flow, considering the difference in the characteristics of the film flows in the two cases.

This result, as well as the results shown in Figures 5 and 6, suggest that the asymptotic relation of Eq. 2, assumed by Henstock and Hanratty, is not correct. However, until an improved understanding of the shear-controlled mass transfer is obtained, the design equations proposed by Henstock and Hanratty can be used to give a good approximation.

DISCUSSION

The constant value of $K^+Sc^{1/2}$ characterizing gas absorption into water at large m^+ is similar to the $K^+ = f(Sc)$ relation found for turbulent mass transfer to a solid wall. Consequently this result is consistent with the notion that liquid phase or gas phase turbulence controls the rate of mass transfer.

Gas phase turbulence is expected to agitate the fluid near the interface, in a manner indicated in Figure 1, through spatial and temporal variations of the shear stress. The magnitude of the turbulent stress fluctuations can be represented by an equation of the form

$$\tau_I = \hat{\tau} \cos(\gamma_t z) e^{i\omega_t t} \tag{22}$$

The magnitude of the velocity fluctuations created in the liquid can be estimated by using the linear momentum equations, and by neglecting any effect of flexing at the interface. The result is very similar to Eq. 13:

$$\hat{v} - \hat{v}_s = -\frac{\hat{\tau}_t y \gamma_t}{\mu(\omega_t/\nu)^{1/2}} \tag{23}$$

The magnitude of the turbulent stress fluctuations can be expected to be about 0.3 $\bar{\tau}_o$ and the dominant turbulent velocity fluctuations at a solid boundary are characterized by a wavelength and frequency (Hanratty et al., 1977) given by

$$\frac{2\pi}{\Upsilon_t} = 100\frac{\nu_G}{v_G^*}, \tag{24}$$

$$\omega_t = 200\pi v_G^{*2}/\nu_G, \tag{25}$$

where $v_G^* = (\bar{\tau}_o/\varrho_G)^{1/2}$. McCready (1984) used these estimates to compare $\hat{\tau}_t\gamma_t/\omega_t^{1/2}$ with $\hat{\tau}_s\alpha^{1/2}/(C - \bar{U}_0)^{1/2}$, defined in Eq. 13. He concluded that, for the experiments described in this paper, interfacial shear stress fluctuations induced by waves will have a much larger effect than those induced by gas phase turbulent velocity fluctuations. Furthermore, the decrease in K^+ with a decrease in m^+ observed for water at $m^+ < 40$ and for glycerine-water for all m^+ is difficult to explain if gas phase turbulence is controlling mass transfer.

Turbulence measurements for highly sheared flows close to solid boundaries would suggest that turbulent normal velocity fluctuations in the liquid close to a highly sheared interface could be important, provided turbulence of the same type as found close to a solid boundary is generated in the liquid near the interface. If such a mechanism were controlling, one would expect the turbulent properties to scale with v^* and ν. The decrease in $K^+ Sc^{1/2}$, for $m + < 40$ observed for water could be explained if the close proximity of the solid wall to the interface impeded the production of turbulence. However, it is very difficult to reconcile the differences found between gas absorption into water and into a water-glycerine solution. Turbulence theory could not explain the larger values of $K^+Sc^{1/2}$ observed for glycerine solutions. It would suggest that both sets of data should give the same value of $K^+Sc^{1/2}$ at large m^+, and that the value of m^+ below which film height is important should not depend on liquid viscosity. Our results therefore suggest that the velocity fluctuations close to the interface that control mass transfer are not described by classical law of the wall arguments.

Consequently, we feel that these controlling velocity fluctuations are related to the wave motion. Support for this is obtained from the similarities of the plots of $K^+Sc^{1/2}$ and of $\overline{h'^2}$ v. m^+. However, it is quite clear that the mass transfer rates cannot be related just to $\overline{h'^2}$. Otherwise, it would be difficult to reconcile the very large effect of liquid viscosity on $\overline{h'^2}$ with its more modest effect on mass transfer rates. It is more than likely that a theory relating mass transfer to wave motion will have to recognize that the small-scale waves, such as are shown in the filtered signal in Figure 8, could be playing a more important role than the larger waves that are more obvious in visual observations.

One way to explain the influence of waves is to argue that the waves create the turbulence in the film and that turbulence near an interface is not described by law of the wall arguments. However, a more appealing explanation is the direct generation of liquid phase motion close to the interface through wave-induced shear stress fluctuations in the gas, as outlined previously in the discussion on the effect of waves. Some support for this as a mechanism that needs to be considered is obtained from calculations carried out by McCready (1984).

Through a computer simulation of the mass transfer at a mobile interface at high Schmidt numbers, the following equation was developed by McCready (1984):

$$K^+Sc^{1/2} = 20(\overline{\beta^{+2}})^{1/4}, \tag{26}$$

where β^+ is the dimensionless gradient of the normal velocity fluctuations in the liquid at the interface:

$$\beta^+ = \left[\frac{dv^+}{dy^+}\right]_s. \tag{27}$$

McCready estimated $(\overline{dv^+/dy^+})_s^2$ from measured wave spectra by using Eq. 13. Because $\hat{\tau}_s$ increases with increasing α (Thorsness

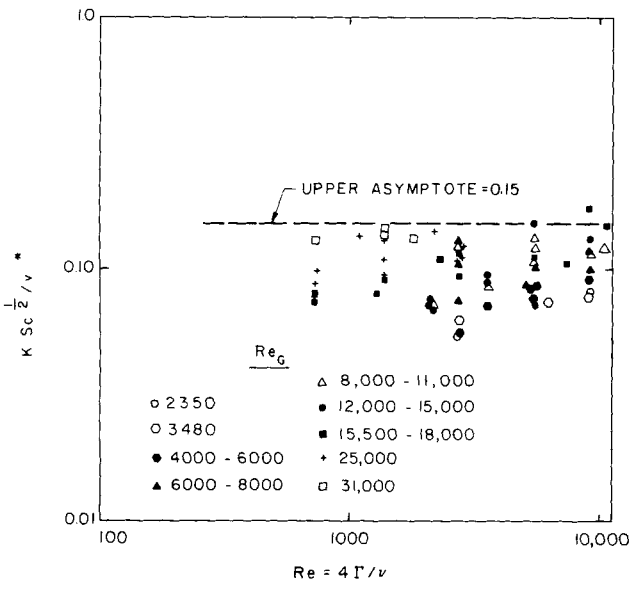

Figure 14. Oxygen absorption results obtained by Henstock and Hanratty (1979) for air and water flowing down a vertical pipe.

et al., 1978) it is expected that the large wave number waves, such as are depicted in the filtered signal shown in Figure 8, are the important ones. McCready approximated these waves by assuming that the surface is covered with a two-dimensional sinusoidal wave pattern with a frequency $N(h_m)$, defined by Eq. 19. The amplitude was estimated by assuming the energy of these waves is that associated with the portion of the wave spectrum over the frequency range of $N(h_m)$ *to* ∞. The wave number was calculated from $N(h_m)$, using the linear dispersion relation. The results of Thorsness et al. (1978) and of Abrams (1984) were used to relate $\hat{\tau}_s$ to the wave amplitude and wave number.

The substitution of values of $\overline{\beta'^2}$ estimated in this way allowed us to calculate K^+ from wave properties. These were found to be close to the measured values for large m^+, but were much larger at smaller m^+. This indicates that fluid motion generated close to an interface by such a mechanism is large enough to be an important factor in controlling mass transfer. However, if it is the controlling factor, then it is also clear that the method outlined above for representing the large wave number waves is an oversimplification.

ACKNOWLEDGMENT

This work was supported by the National Science Foundation under Grant NSF CPE 82-19065 and by the Shell Companies Foundation.

NOTATION

a = wave amplitude
B = channel height
C = wave speed
c = concentration
c^* = equilibrium concentration
D = parameter defined by Eq. 12
h = film height
h' = film height fluctuation $= h - \bar{h}$
K = mass transfer coefficient
L = length between two sampling points
m = time averaged film height $= \bar{h}$
n = frequency, Hz
$P(h)$ = probability density function for film height
Re = liquid film Reynolds number $= 4\Gamma/\mu_L$
Re_G = gas Reynolds number $= (B - m)V_G/\nu_G$
Sc = Schmidt number
t = time
u = wave-induced variation of liquid velocity in the x direction
U = time-averaged velocity in the liquid
U_o = time-averaged liquid velocity at $y = m$
U_t = time-averaged liquid velocity at the interface
v = wave-induced variation of liquid velocity in the y direction
V_G = bulk averaged velocity of the gas
v^* = friction velocity for the liquid $= (\bar{\tau}_o/\varrho)^{1/2}$
v_G^* = friction velocity for the gas $= (\bar{\tau}_o/\varrho_G)^{1/2}$
$W_h(n)$ = spectral density function for the fluctuations in film height
x = coordinate in the direction of mean flow
y = coordinate in a direction perpendicular to the channel wall
z = coordinate in the spanwise direction

Greek Letters

α = wave number $= 2\pi/\lambda$
β = gradient of the normal velocity component evaluated at the interface
Γ = volumetric flow rate per unit width
Υ_t = wave number characterizing the variation of the gas phases shear stress fluctuations in the z direction
η = surface location $= h - m$
λ = wavelength
μ = liquid viscosity
ν = kinematic viscosity of the liquid
ν_G = kinematic viscosity of the gas
ϱ = liquid density
ϱ_G = gas density
$\bar{\tau}_o$ = average shear stress at $y = m$
τ_s = shear stress variations at the interface induced by waves
τ_t = shear stress fluctuations at the interface caused by gas phase turbulence
ω_t = frequency, in radians per record, of the dominant gas phase turbulent fluctuations at the interface

Other Symbols

$\hat{}$ = indicates the complex amplitude of wave-induced variation or of a characteristic turbulent flutuation
$+$ = quantity made dimensionless using the kinematic viscosity and the friction velocity
$-$ = time average
$||$ = magnitude of the complex amplitude

LITERATURE CITED

Abrams, J., "Turbulent Flow Over Small Amplitude Solid Waves," Ph.D. Thesis, Univ. of Illinois, Urbana (1984).

Chung, D. K., and A. F. Mills, "Experimental Study of Gas Absorption into Turbulent Falling Films of Water and Glycol-Water Mixtures," *Letters Heat Mass Trans.*, **1**, 43 (1974).

Hanratty, T. J., "Interfacial Instabilities Caused by Air Flow Over a Thin Liquid Layer," *Waves on Fluid Interfaces*, Richard E. Meyer, Ed., Academic Press, New York, 221 (1983).

Hanratty, T. J., L. G. Chorn, and D. T. Hatziavramides, "Turbulent Fluctuations in the Viscous Wall Region for Newtonian and Dray Reducing Fluids," *The Physics of Fluids*, **20**, S112 (1977).

Henstock, W. H., and T. J. Hanratty, "Gas Absorption by a Liquid Layer Flowing on the Wall of a Pipe." *AIChE J.*, **25**, 122 (1979).

——, "The Interfacial Drag and the Height of the Wall Layer in Annular Flows," *AIChE J.*, **22**, 990 (1976).

Henstock, W. H., "The Effect of a Concurrent Gas Flow on Gas-Liquid Mass Transfer," Ph.D. Thesis, Univ. of Illinois, Urbana (1977).

Kamei, S., and J. Oishi, "Mass and Heat Transfer in a Falling Liquid Film of Wetted Wall Tower," *Mem. Fac. Eng. Kyoto Univ.*, **17**, 277 (1955).

Mattingly, G. E., "Experimental Study of Wind Effects on Reaeration," *J. Hydraulics Div. ASCE*, **103** (HY3), 311 (1977).

Maxwell, W. H. C., and E. R. Holley, "A Method for Deaerating Water," *J. Hydraulics Div. ASCE*, **95** (HY1), 577 (1969).

McCready, M., "Mechanisms of Gas Absorption at a Sheared Gas-Liquid Interface," Ph.D. Thesis, Univ. of Illinois, Urbana (1984).

Miya, M., "Properties of Roll Waves," Ph.D. Thesis, Univ. of Illinois, Urbana (1970).

Suzanne, C., "A Study of Gas-Liquid Stratified Flows," Thèse de Docteur-Ingenieur, Université Paul Sabatier de Toulouse (1977).

Thorsness, C. B., P. E. Morrisroe, and T. J. Hanratty, "A Comparison of Linear Theory with Measurements of the Variation of Shear Stress Along a Solid Wave," *Chem. Eng. Sci.*, **33**, 579 (1978).

Tsacoyannis, Y., "A Study of Gas Absorption into Liquids in Turbulent Stratified Flows," Thèse de Docteur-Ingenieur, Université Paul Sabatier de Toulouse (1976).

Manuscript received Oct. 16, 1984, and revision received Mar. 13, 1985.